



Rotational Microorganism Magneto-hydrodynamic Nanofluid Flow with Lorentz and Coriolis Force on Moving Vertical Plate

Shweta Mishra¹ · Hiranmoy Mondal¹

Accepted: 12 December 2023 / Published online: 11 January 2024

© The Author(s), under exclusive licence to Springer Science+Business Media, LLC, part of Springer Nature 2024

Abstract

The electrically conducting rotational microbial nanofluid with Coriolis and Lorentz force over a moving plate in the vertical direction with the velocity ratio at the boundary condition is considered in this article. The modeled equations are converted into nonlinear ordinary with boundary conditions by using some similarity transformation. The governing equations are numerically solved by a bivariate spectral quasi-linearization technique. The influence of the numerous parameters is analyzed graphically for the velocity, thermal, solutal, and microorganism profiles. The collection points and error graph are also included in the manuscript for justifying the technique. The increasing values of the magnetic field parameters reduce the flow profile, and similar behavior is observed for the velocity ratio and buoyancy ratio parameters. The microbial profile is enhanced with the increment of Hall current, Brownian motion for microbial, and buoyancy ratio constraints. The comparison graph was also included, and the results are in favor of our model.

Keywords Rotational Nanofluid · BSQLM · Oxytactic microorganisms · bio-convection · Vertical Plate · Hall Current

Nomenclature

List of Symbols

u, v, w	Fluid velocity (m s^{-1})
x, y, z	Cartesian coordinates
T	Temperature (K)
M	Magnetic field parameter (T)
C	Fluid concentration (moles = kg)
D_n	Microbial Brownian diffusion (m^2s^{-1})
n	Fluid microbial concentration (moles = kg)
N	Hall parameter
g_t	Acceleration due to gravity ($\text{m} = \text{s}^2$)
D_B	Solutal Brownian diffusion (m^2s^{-1})
f	Dimensionless stream function
k	Thermal conductivity ($W = \text{mK}$)
C_s	Concentration susceptibility
Sc	Schmidt number
Sh	Local Sherwood number
ul	Dimensionless velocity
Nr	Buoyancy ratio parameter

Rb	Bio-convection Rayleigh number
Le	Lewis number
S	Velocity ration
Ec	Eckert number
Pr	Prandtl number
C	Nanoparticle volume fraction
E_1	Local electric parameter
Gr	Grashof number
Nt	Thermophoresis parameter
Nb	Brownian motion parameter
Np	Bio-convection Brownian motion parameter
Re	Reynolds number
D_T	Thermophoretic diffusion coefficient (m^2s^{-1})
Sb	Bio-convection Schmidt number
Pb	Bio-convection Peclet number
cp	Effective specific heat coefficient of fluid ($J = \text{kg K}$)
b	Chemotaxis constant

Greek symbols

β_t	Thermal expansion coefficient
ϕ	Dimensionless nanoparticle volume fraction
β_c	Volumetric expansion coefficient
ψ	Stream function
α	Wall thickness parameter
σ	Electrical conductivity (S m^{-1})
η	Similarity independent variable

✉ Shweta Mishra
shweta9935@gmail.com

¹ Department of Applied Mathematics, Maulana Abul Kalam Azad University of Technology, Haringhata, Nadia -741249, India

$(\rho c)_f$	Heat capacity of nanofluid
ν	Kinematic viscosity ($\text{m}^2 \text{s}^{-1}$)
μ	Dynamic viscosity (kg m s^{-1})
τ	Dimensionless time
ρ	Density (kg m^{-3})
$(\rho c)_p$	Effective heat capacity of the nanoparticle
ξ	Rotational parameter

1 Introduction

The applications of the magneto-hydro-dynamic with controlling heat and mass transfer over a continuously extending sheet, reactors for nuclear, generators of power, understating plasma, and extracting the energy of geothermal grab the eyeballs of many researchers. The involvement of magneto-hydro-dynamic flow of convective induced the Hall current in the magnetic and electric field from the normal direction. The impact of Hall current cannot be ignored due to the strong magnetic field or/and low density of the ionized gasses. The flow of convective utilizing magneto-hydro-dynamic was analyzed in [1–11], having a strong magnetic field passing over a vertical flat plate which is semi-infinite. There is some researcher who discussed this with vertical plate [12–17] with other parameters.

Due to the broader applications in the jet motors, mass spectrometry, computer floppy drive, domain of nutrition processing, turbine systems, generation of electric power, and rotational fluids are gaining the attention of researchers. Some researchers [18–26] studied the rotational body with the Hall current, considering the presence of a magnetic field very high. While [27] discussed the impact of Hall current combined with a strong magnetic field, with the free stream flow over a horizontally moving plate, and [28] studied the flow of rotational fluid of secondary grade for heat transfer with Hall current passing over a porous media. Several scenarios of the rotating disk concept have been studied by researchers, including the use of ferrofluid [29], Darcy-Forchheimer fluid [30], Stefan Blowing on Rener-Rivlin flow [31], and MHD flow with radiative heat [32]. Additionally, some authors have considered entropy optimization on a rotating disk [33, 34]. Several authors [35–37] have analyzed the effects of different parameters on micropolar fluids.

To emphasize the energy system by thermal conductivity, researchers used several methods in the heat mass transmission, and then microorganisms incorporated in bio-convection nanofluids grabbed their attention. The movements of these microorganisms in the nanofluid modernize as the bio-convection nanofluid, which is in higher dimension. Many researchers have been working on controlling heat, momentum, and mass transmission rates of nanofluids and microbial microorganisms [37–41].

Analysis of mass and heat transmission for convective borderline circumstances is significant for reactors of atoms and turbines of gasses, accompanied by exchangers of heat into the industries. Nanofluids are integrated into bio-medical disciplines due to their solicitation in the labeling of cancerous tissues, cancer therapeutics, magnetic resonance imaging (MRI), and magnetic resonance, nano-drug delivery, nano-cryosurgery, localized therapy, and bacteriostatic activity, which was investigated in [42]. The impact of viscous dissipation for convection nanofluid flow via vertical surface was observed by many researchers. The nanofluid flow of mixed convection with the presence of different parameters is numerically instigated in [43–46].

The application of the Lorentz force, a magnetic field, has led to numerous modern applications such as plastic material assembly, glass fiber production, fluid engineering, and disease treatment. Several researchers have discussed the use of the Lorentz force in various domains [47–50]. For instance, the Coriolis force has been studied in geophysics, astrophysics problems, and centrifugal reactors of bio [48], while its impact on the stretching surface of the nanofluid of Prandtl was analyzed by another researcher [49].

In scientific studies, different types of rotating nanofluids have been analyzed for their properties. One study in [50] looked at the microorganism in rotating nanofluid on the Riga plate using non-Fourier flux of heat and binary chemical reaction. Another study in [51] investigated the importance of Lorentz and Coriolis forces on rotating Boger nanofluid. While [52] researched the rotational nanofluid of Carreau-Yasuda with the Coriolis force, including gyrotactic microorganisms, while [53] analyzed the impact of these forces on the Maxwell nanofluid.

The bivariate spectral quasi-linearization method is very useful for explaining the nonlinear differential equations having two variables. Due to its accuracy and time-consuming nature, researchers are using this for different studies [54, 55].

The above literature assessment shows that very few researchers have studied the combination of microorganisms with Lorentz and Coriolis forces on a vertically placed plate in rotating fluid with the effect of Hall current. This article examined the influence of rotational nanofluid flows with Coriolis and Lorentz force on microorganisms and viscous dissipation on a motile, semi-infinite vertical plate. To solve the governing partial differential equations along with the boundary conditions, we used suitable similarity constraints to transform them into ordinary differential equations. We utilize the Bivariate Spectral Quasi Linearization Method (BSQLM) to solve the improved boundary equations along the momentum, energy, solute, and microbial equations. Moreover, we also analyzed the impact of some other constraints on the assumed model.

2 Mathematical Analysis

A rotational viscous dissipative nanofluid flow on a vertically placed mobile plate accompanied by the magnetic field and motile microorganism is considered in this investigation. The Coriolis and Lorentz forces generated by applying the strong magnetic field on the vertically placed semi-infinite plate, from the buoyancy forces engendered from the concept of coupled occurrence of heat and species-concentration, into an incompressible, steady, and electrically conducting magneto-hydro-dynamic bio-convective rotational nanofluid.

Figure 1 reflects the physical demonstration of our assumed model; the rectangular coordinates are $x, y,$ and $z,$ while the flow constituents are $u, v,$ and w to the corresponding orders. A semi-infinite vertically placed flat plate is considered for our model at the plane $x-z,$ which traces z by velocity U_1 into an electrically conducted, viscous dissipative rotational nanofluid stream, spinning with the uniform angular velocity Ω_0 in the y -axis direction incorporated with the oxytaxis microbes. While the persistent flow of free stream U_2 is assumed comparable in the z -axis direction, and the strong force field B_0 is considered on the plate normally beside the y -axis, and thus, the impact of Hall currents is quite influential since the Reynolds numerals of the magnetic field are tiny, i.e., $\mu_0 \bar{V}L \ll 1;$ here characteristic length is $\bar{L},$ characteristic flow is $\bar{V},$ and magnetic permeability is $\mu_0,$ as referenced in [27, 56]. The mathematical formulation of our model can be written as follows:

The continuity equation

$$\nabla \cdot V = 0. \tag{1}$$

The equation of momentum

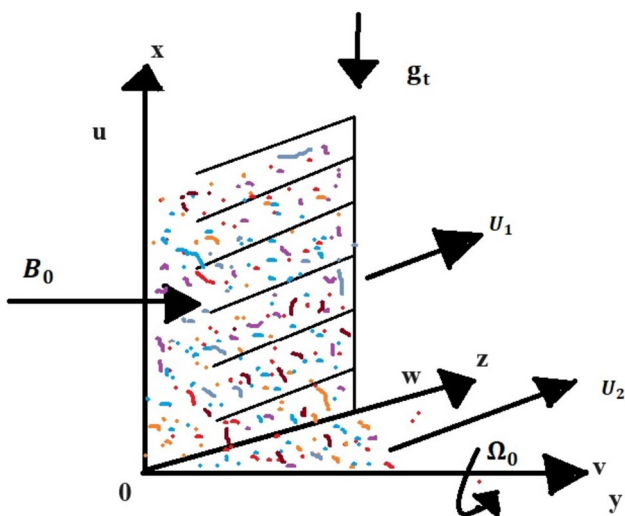


Fig. 1 Graphical demonstration of the model

$$(\nabla \cdot \nabla)V + 2\Omega_0 \times V + \frac{1}{\rho} \nabla p - \nu \nabla^2 V - \frac{1}{\rho} (J \times B) - \frac{\gamma}{\rho} \beta (1 - C_\infty) (T - T_\infty) + \frac{(\rho_p - \rho_f)}{\rho_f} \frac{\gamma}{\rho_f} (C - C_\infty) + \frac{\gamma}{\rho_f} \frac{(\rho_p - \rho_f)}{\rho_f} (n - n_\infty) = 0. \tag{2}$$

The equation of energy

$$(\nabla \cdot \nabla)T - \alpha_m \nabla^2 T - \tau \left[D_B \nabla T \nabla C + \frac{D_T}{T_\infty} \nabla T \cdot \nabla T + D_n \nabla T \nabla n \right] - \frac{\nu}{c_p} [(\nabla V)^2] - \frac{1}{\rho} (J \times B) \cdot (V^2) = 0 \tag{3}$$

The equation of mass concentration

$$(\nabla \cdot \nabla)C - D_B \nabla^2 C - \frac{D_T}{T_\infty} \nabla^2 T = 0 \tag{4}$$

The equation of microorganism concentration

$$(\nabla \cdot \nabla)n - \nabla \cdot \left(\frac{b w_c}{\Delta C} (n \nabla C) \right) - D_n \nabla^2 n - \frac{D_T}{T_\infty} \nabla^2 T = 0 \tag{5}$$

Here, the fluids flow vector is represented by $V(u, v, w),$ while the magnetic field implemented on the plate is denoted by $B(0, B_0, 0).$

The induced Hall current is given by a generalized Ohm’s law, as referenced in [17, 27, 47],

$$J = \frac{\sigma}{1 + \left(\frac{\omega}{\nu_e} \right)^2} \left[E + (V \times B) - \frac{J \times B}{en_e} \right] \tag{6}$$

The stimulating current vector $J = (J_x, J_y, J_z),$ velocity vector $V,$ and ferocity of tense field E, B magnetic-induction, $1/ne$ Hall factor, $N = \omega/\nu_e$ Hall parameter, n_e electron number density, ν_e frequency of electron-atom collision, and ω

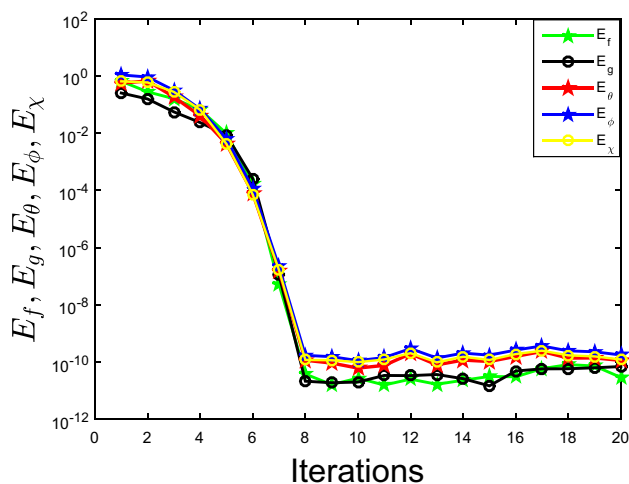


Fig. 2 Residual norm iterations on variation

electron cyclotron. The very large ω/ν_e affects the electromagnetic field, which affects ions and electrons both for relative drift between these with the neutrals; this is known as ion slip; in addition, it is usually insignificant for highly ionized gasses.

Moreover, the equivalence of Maxwell's with the Hartmann numeral

$$\nabla \times \mathbf{H} = \mathbf{J}; \quad \nabla \times \mathbf{E} = 0; \quad \nabla \cdot \mathbf{B} = 0. \quad (7)$$

Since the electrical field from outside is not included and can be assumed as zero; thus, Eq. (6) can be rewritten as follows, as referenced in [17, 47]:

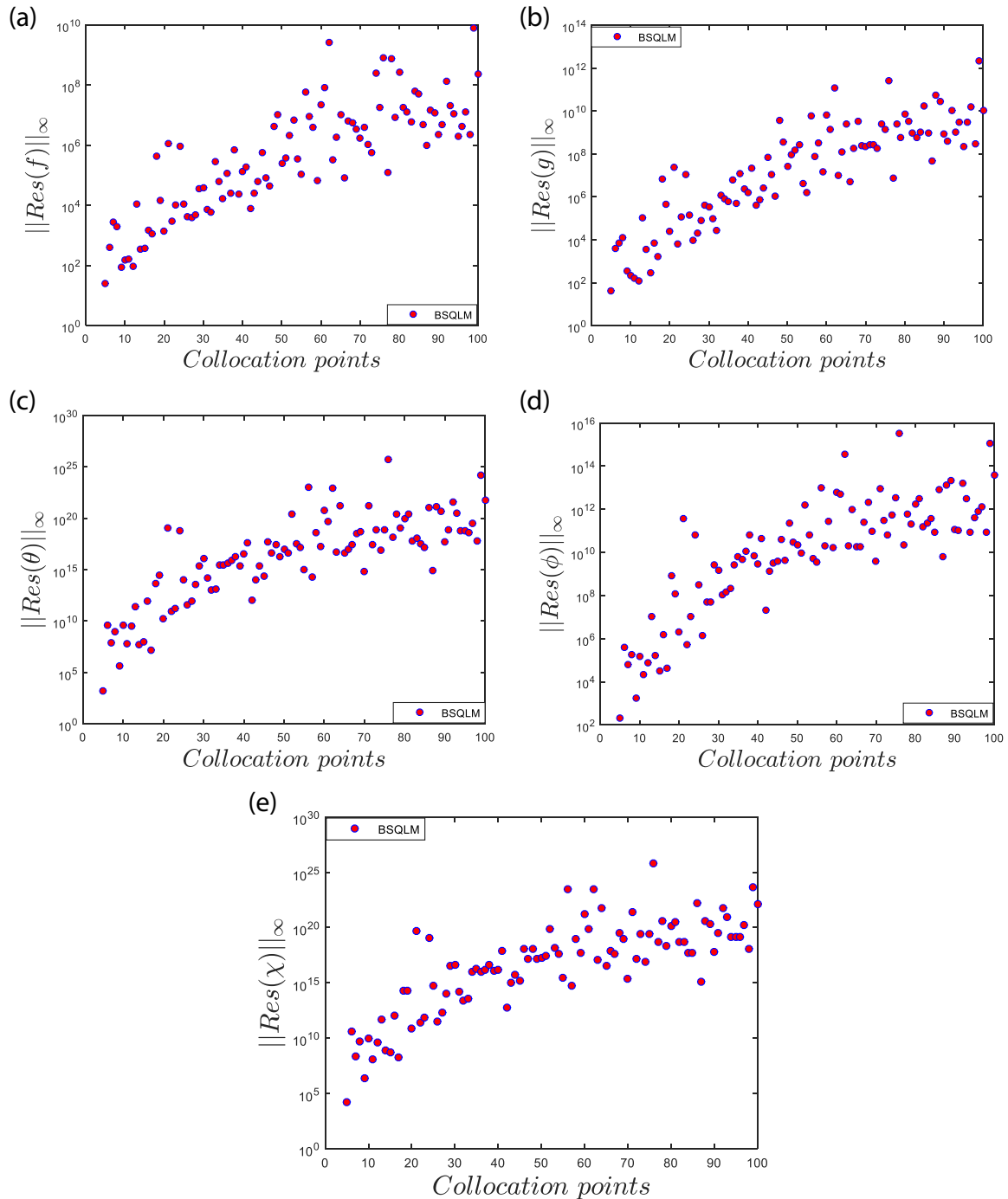


Fig. 3 Collocation points of (a) principal velocity, (b) subordinate velocity, (c) heat profile, (d) concentration profile, and (e) microbial contour

$$J = \frac{\sigma}{1 + \left(\frac{\omega}{v_e}\right)^2} \left[(V \times B) - \frac{J \times B}{en_e} \right]. \tag{8}$$

In this investigation, we assumed that the ion slip and pressure of thermo-electric are insignificant with electrical and viscous dissipation of the fluid. The cross flow induced in the z -direction is generated by the Coriolis force. Moreover, there are no changes in the flow, mass, and heat transmission on the assumed semi-infinite vertically placed plate in this direction:

$$J_x = \frac{\sigma B_0}{1 + N^2} [Nu - w]; J_y = 0; \text{ and } J_z = \frac{\sigma B_0}{1 + N^2} [u + Nw]. \tag{9}$$

The flow heat, solute, and microbes are considered as persistent on the wall and denoted as $T_w, C_w,$ and $n_w,$ and from the wall, which is the free stream, they are denoted as $T_\infty, C_\infty,$ and n_∞ correspondingly. The Hall currents and Coriolis energy enhance a force toward the y -axis by generating the cross flow in the z -axis. The electromagnetic equations of Maxwell with the spinning flow of our assumed model, as referenced in [24, 47], are transcribed as

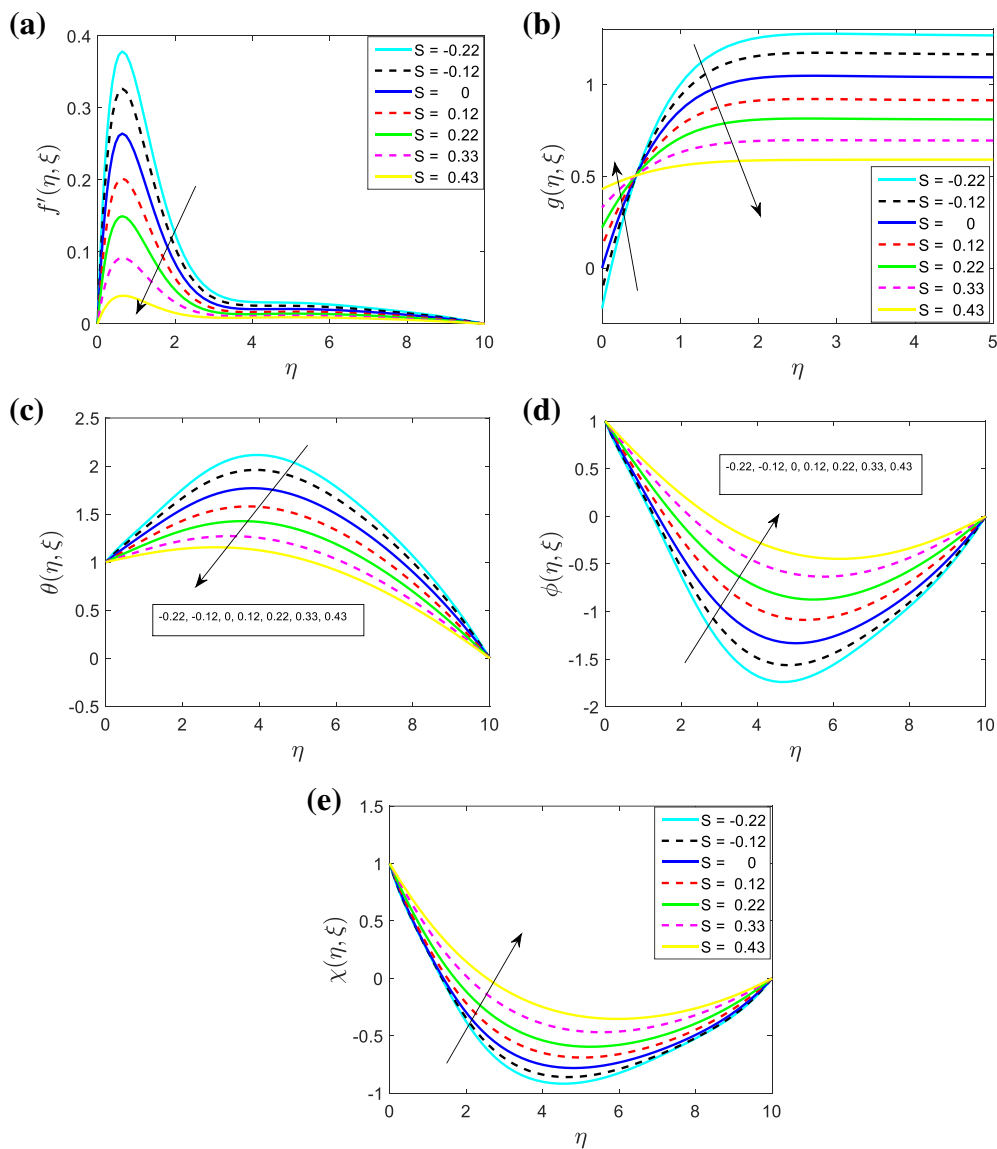


Fig. 4 Influence of S on (a) principal velocity and (b) subordinate velocity. Repercussion of S on (c) heat profile, (d) concentration profile, and (e) microbial contour

$$\frac{\partial u}{\partial x} + \frac{\partial v}{\partial y} = 0, \tag{10}$$

$$u \frac{\partial u}{\partial x} + v \frac{\partial u}{\partial y} + 2\Omega_0 w = -\frac{1}{\rho} \frac{\partial p}{\partial x} + v \frac{\partial^2 u}{\partial y^2} - \frac{\sigma B_0^2}{\rho(1+N^2)}(u + Nw) + g_t \beta(1 - C_\infty)(T - T_\infty) - \frac{(\rho_p - \rho_f)}{\rho_f} g_t (C - C_\infty) - \frac{\gamma g_t (\rho_p - \rho_f)}{\rho_f} (n - n_\infty). \tag{11}$$

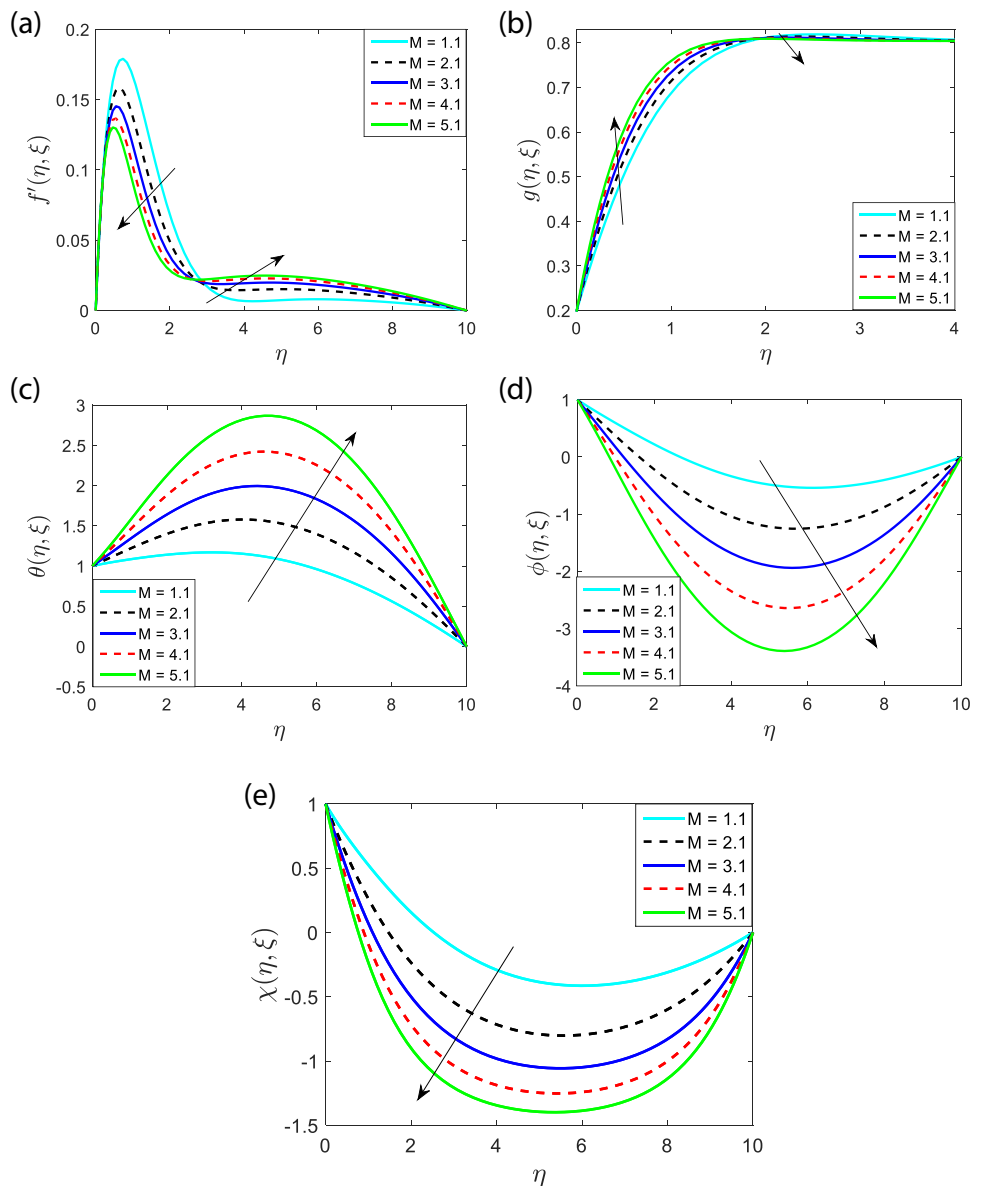
$$u \frac{\partial w}{\partial x} + v \frac{\partial w}{\partial y} - 2\Omega_0 w = -\frac{1}{\rho} \frac{\partial p}{\partial z} + v \frac{\partial^2 w}{\partial y^2} - \frac{\sigma B_0^2}{\rho(1+N^2)}(w - Nu) \tag{12}$$

$$u \frac{\partial T}{\partial x} + v \frac{\partial T}{\partial y} = \alpha_m \frac{\partial^2 T}{\partial y^2} + \tau \left[D_B \frac{\partial T}{\partial y} \frac{\partial C}{\partial y} + \frac{D_T}{T_\infty} \left(\frac{\partial T}{\partial y} \right)^2 + D_n \frac{\partial T}{\partial y} \frac{\partial n}{\partial y} \right] + \frac{v}{c_p} \left[\left(\frac{\partial u}{\partial y} \right)^2 + \left(\frac{\partial w}{\partial y} \right)^2 \right] + \frac{\sigma B_0^2}{\rho(1+N^2)}(u^2 + w^2) \tag{13}$$

$$u \frac{\partial C}{\partial x} + w \frac{\partial C}{\partial z} = D_B \frac{\partial^2 C}{\partial z^2} + \frac{D_T}{T_\infty} \frac{\partial^2 T}{\partial z^2}, \tag{14}$$

$$u \frac{\partial n}{\partial x} + w \frac{\partial n}{\partial z} + \frac{bW_c}{\Delta C} \frac{\partial}{\partial z} \left(n \frac{\partial n}{\partial z} \right) = D_n \frac{\partial^2 n}{\partial z^2}, \tag{15}$$

Fig. 5 Influence of M on (a) principal flow and (b) subordinate flow. Impact of Hartmann number on (c) heat profile and (b) solute profile. (e) Influence of Hartmann number on micro-organisms profile



The Coriolis and Lorentz forces are considered for balancing the pressure in the fluid toward the y and x axes, $-\rho^{-1}\rho_z$ and $-\rho^{-1}\rho_x$, respectively, and are written as

$$-\frac{1}{\rho} \frac{\partial p}{\partial x} = 2\Omega_0 U_2 + \frac{\sigma B_0^2}{\rho(1+N^2)} NU_2, \quad -\frac{1}{\rho} \frac{\partial p}{\partial z} = \frac{\sigma B_0^2}{\rho(1+N^2)} U_2 \tag{16}$$

The borderline conditions for Eqs. (10)–(15) are given as

$$\begin{aligned} u(x, 0) = 0, v(x, 0) = 0, w(x, 0) = U_1, \\ T = T_w, C = C_w, n = n_w \text{ at } y = 0, \\ w = U_2, u, v = 0, T = T_\infty, C = C_\infty, n = n_\infty, \text{ as } y \rightarrow \infty. \end{aligned} \tag{17}$$

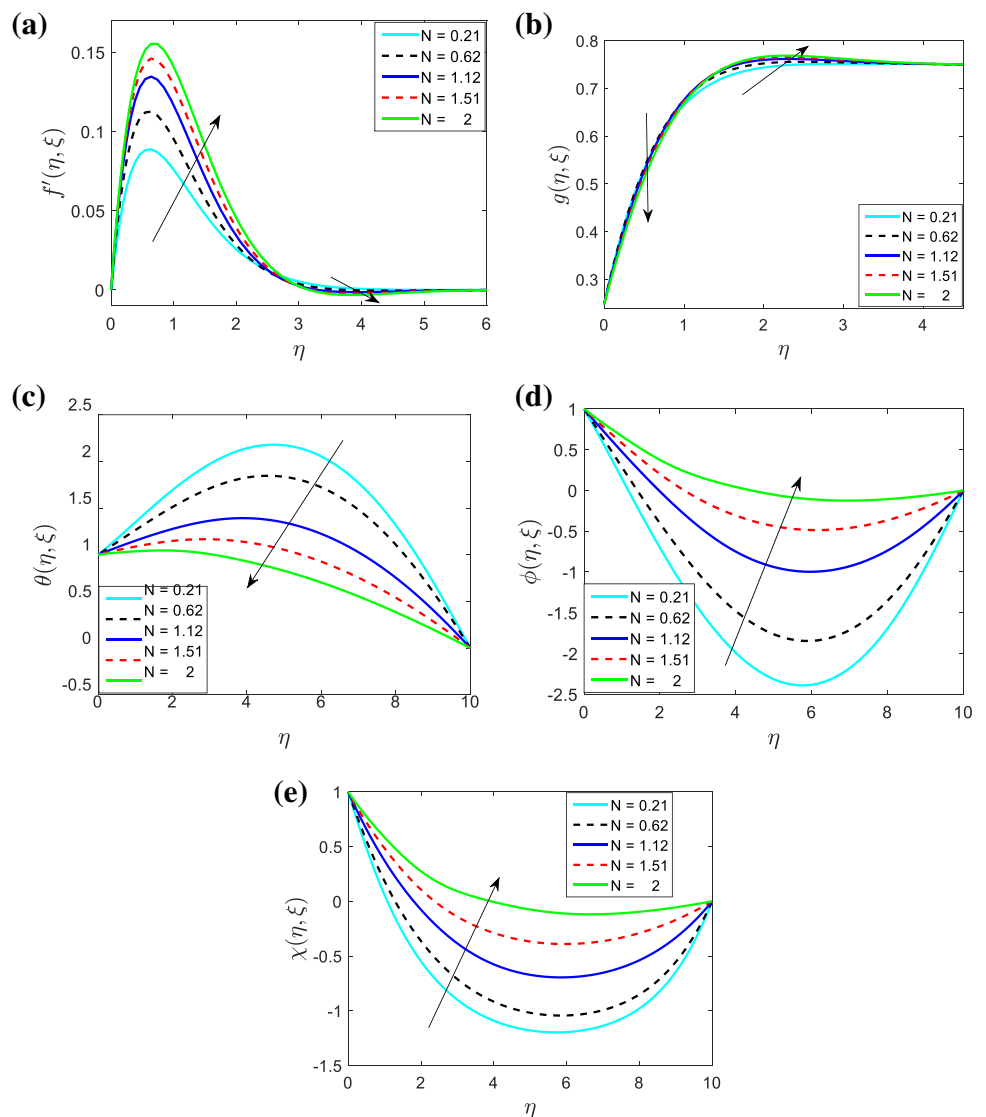
Here, base fluid density is denoted by ρ , kinematic viscosity is ν , fluid’s electrical conductivity is σ , the gravitational

acceleration by g_p , Hall parameter is N , expansion of volumetric coefficient by β , the nanoparticles density is ρ_p and nanofluid density is ρ_f microbes density is ρ_m , microbes average volume by γ , microbes thermal diffusivity by α_m , τ is the heat capacitance for nanoparticles to the base fluid ratio, the thermophoretic diffusion by D_T , solutal Brownian diffusion quantity is D_B , microorganism Brownian diffusion by D_m , the extreme cell spinning rapidity (bWc is considered to be uniform) by w_c , and chemotaxis constant by b .

3 Transformation of Equations

To transform the assumed system of equations of our model specified in Eqs. (10)–(15), subsequent similarity transformations are considered:

Fig. 6 Influence of Hall current on (a) principal flow, (b) subordinate flow, (c) heat profile, (d) solute profile, and (e) microorganisms profile



$$\eta = y\sqrt{\frac{U_0}{\nu x}}, \psi = \sqrt{U_0\nu x}f(\xi, \eta), \xi = \frac{\Omega x}{U_0}$$

$$u = U_0f'(\xi, \eta), v = -\sqrt{\frac{\nu\Omega}{\xi}}\left[\xi\frac{\partial f}{\partial \xi} + f - \frac{1}{2}\eta f'\right], \tag{19}$$

$$w = U_0g(\xi, \eta), U_0 = U_1 + U_2, S = \frac{U_1}{U_0}$$

Equations (11)–(15), with the help of Eqs. (16), (18)–(19), considering borderline conditions from Eq. (17), are renovated into the subsequent boundary value problem:

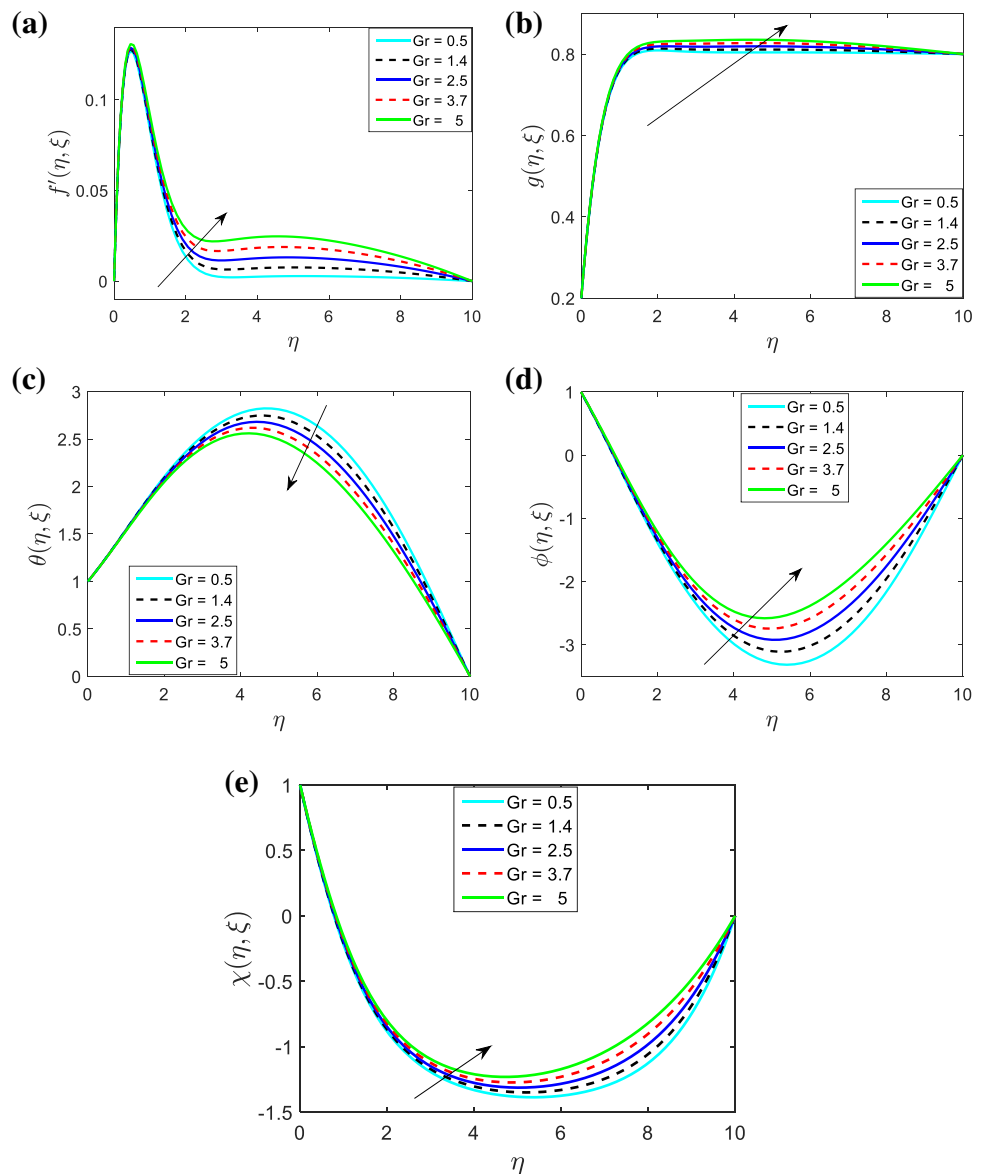
$$\theta(\xi, \eta) = \frac{T - T_\infty}{T_w - T_\infty}, \phi(\xi, \eta) = \frac{C - C_\infty}{C_w - C_\infty}, \chi(\xi, \eta) = \frac{n - n_\infty}{n_w - n_\infty} \tag{18}$$

$$f''' + ff'' - f'^2 - 2\xi g + 2\xi(1 - S) - \frac{M}{1 + N^2}\xi(f' - N + NS + Ng) \tag{20}$$

The flow constituents $u = \frac{\partial \psi}{\partial z}$ and $w = -\frac{\partial \psi}{\partial x}$ and $v = -\frac{\partial \psi}{\partial x}$ are given as

$$+ \frac{Gr}{Re^2}\xi(\theta - Nr\varphi - Rb\chi) - \xi\left(f'\frac{\partial f'}{\partial \xi} - f''\frac{\partial f}{\partial \xi}\right) = 0.$$

Fig. 7 Influence of *Gr* on (a) principal flow, (b) subordinate flow, (c) heat profile, (d) solute profile, and (e) microorganisms profile



$$\begin{aligned}
 &g'' + fg' - gf' + 2\xi f' \\
 &- \frac{M}{1 + N^2} \xi [g + S - Nf' - 1] \\
 & - \xi \left(f' \frac{\partial g}{\partial \xi} - g' \frac{\partial f}{\partial \xi} \right) = 0
 \end{aligned} \tag{21}$$

$$\begin{aligned}
 &\theta'' + Pr f \theta' + Pr(Nb\theta' \varphi' + Nt\theta'^2 + Nt\theta' \chi') + PrEc(f'^2 + g'^2) \\
 & + \frac{M}{1 + N^2} PrEc\xi(f'^2 + g'^2) - Pr \xi \left(f' \frac{\partial \theta}{\partial \xi} - \theta' \frac{\partial f}{\partial \xi} \right) = 0
 \end{aligned} \tag{22}$$

$$\varphi'' + Scf \varphi' + \frac{Nt}{Nb} \theta'' - Sc\xi \left(f' \frac{\partial \varphi}{\partial \xi} - \varphi' \frac{\partial f}{\partial \xi} \right) = 0 \tag{23}$$

$$\begin{aligned}
 &\chi'' + Sbf \chi' - Pb[\chi' \varphi' + (\tau_0 + \chi)\varphi''] \\
 & + \frac{Nt}{Np} \theta'' - Sb\xi \left(f' \frac{\partial \chi}{\partial \xi} - \chi' \frac{\partial f}{\partial \xi} \right) = 0
 \end{aligned} \tag{24}$$

Here, the primes are the differentiation w. r. to η . The transformed boundary conditions of the corresponding borderline situations (7) are

$$\begin{aligned}
 &f'(\xi, \infty) \rightarrow 0, \quad f'(\xi, 0) = 0, \quad f(\xi, 0) = 0, \\
 &g(\xi, 0) = S, \quad g(\xi, \infty) = 1 - S, \\
 &\theta(\xi, \infty) \rightarrow 0, \quad \theta(\xi, 0) = 1, \\
 &\varphi(\xi, \infty) \rightarrow 0, \quad \varphi(\xi, 0) = 1, \\
 &\chi(\xi, \infty) \rightarrow 0, \quad \chi(\xi, 0) = 1.
 \end{aligned} \tag{25}$$

The parameters defined in the associated equations with borderline conditions are as follows.

Here, the modified Hartmann number $M = \frac{\sigma B_0^2}{\rho \Omega}$, the Grashof number $Gr = \frac{(1 - C_\infty) \beta (T_w - T_\infty)}{U_0 \Omega}$, $Re = \frac{U_0 x}{\nu}$, Reynolds number, ξ is the rotational parameter, the buoyancy ratio parameter $Nr = \frac{(\rho_p - \rho_f)(C_w - C_\infty)}{(1 - C_\infty) \rho \beta (T_w - T_\infty)}$, the bio-convection Rayleigh number $Rb = \frac{\gamma (\rho_m - \rho_f) (n_w - n_\infty)}{\beta \rho_f \rho_f^\infty (1 - C_\infty) (T_w - T_\infty)}$, the Schmidt number $Sc = \frac{\nu}{D_B}$, the Brownian motion parameter $Nb = \frac{\tau D_B (C_w - C_\infty)}{\nu}$, the Prandtl number $Pr = \frac{\nu}{\alpha}$, the bio-convection Brownian motion parameter $Np = \frac{\alpha \tau D_n (n_w - n_\infty)}{\nu}$, the thermophoresis parameter $Nt = \frac{\tau D_T (T_w - T_\infty)}{\nu T_\infty}$, the bio-convection Schmidt number $Sb = \frac{\nu}{D_n}$, the constant microorganisms concentration difference parameter is $\tau_0 = \frac{n_\infty}{n_w - n_\infty}$, the Reynolds number $Re_x = \frac{U_0 x}{\nu}$, and the velocity ratio $S = \frac{U_1}{U_0}$, bio-convection Peclet number $Pb = \frac{b w_c}{D_n}$.

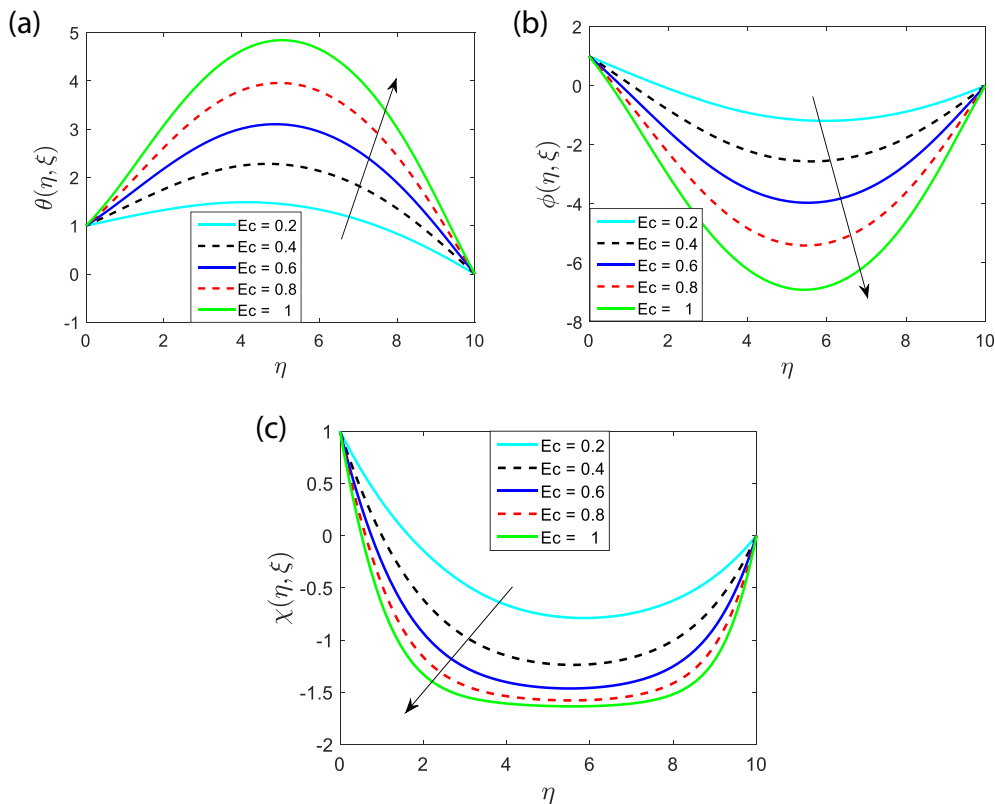


Fig. 8 Influence of Eckert number on (a) heat profile, (b) solute profile, and (c) microbial profile

4 Coefficients of Heat Mass and Momentum

The coefficients of local skin friction toward the horizontal and free stream directions are

$$Sh_x = \frac{xq_w}{D_B(C_w - C_\infty)} = -Re_x^{\frac{1}{2}}\phi'(\xi, 0), \text{ where } q_m = -D_B \left. \frac{\partial C}{\partial y} \right|_{y=0}, \tag{28}$$

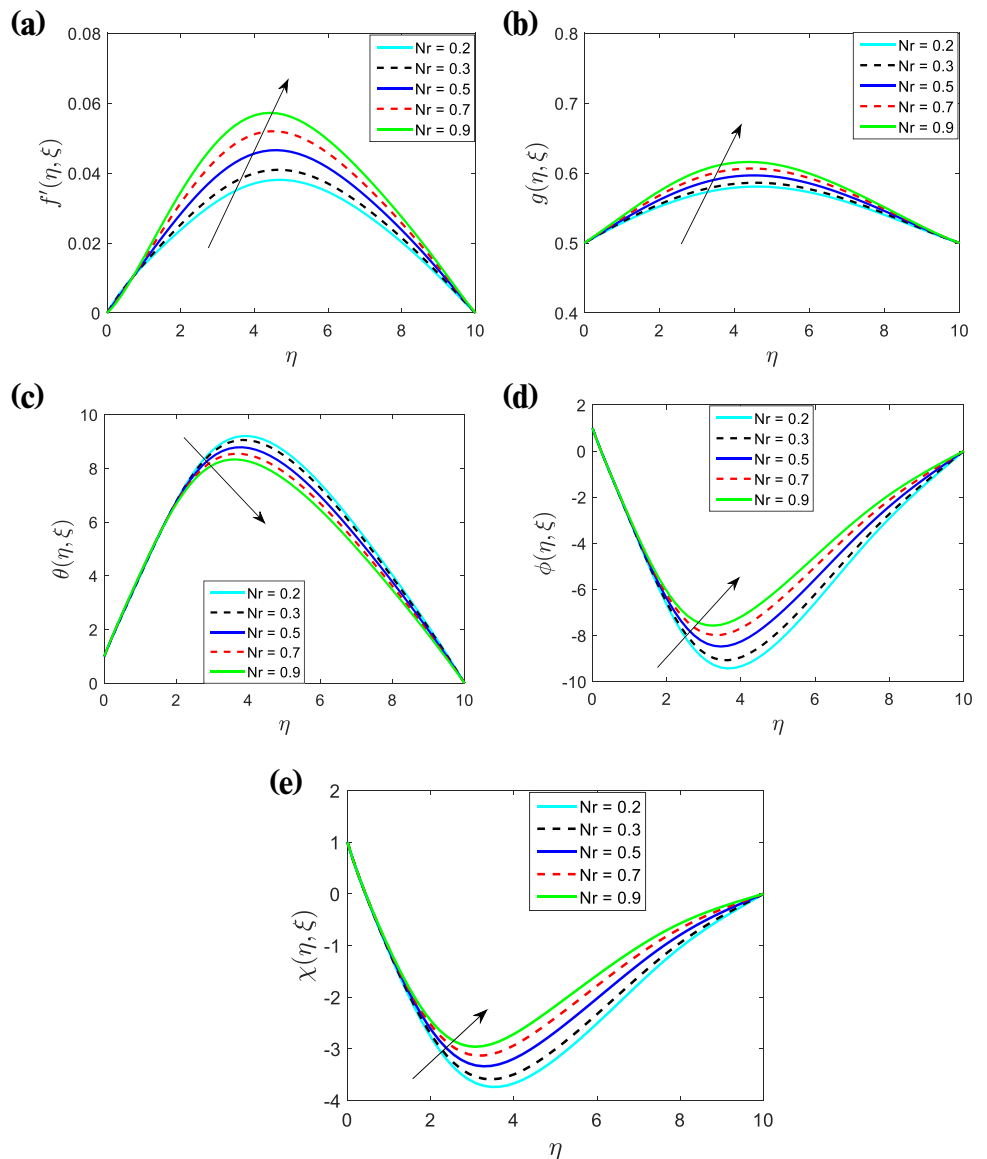
$$C_{fx} = \frac{\tau_{wx}}{\frac{1}{2}\rho U_0^2} = 2(Re_x)^{-\frac{1}{2}}f''(\xi, 0), \text{ where } \tau_{wx} = \mu \left. \frac{\partial u}{\partial y} \right|_{y=0} \text{ and } C_{fy} = \frac{\tau_{wy}}{\frac{1}{2}\rho U_0^2} = 2(Re_y)^{-\frac{1}{2}}g'(\xi, 0), \text{ where } \tau_{wz} = \mu \left. \frac{\partial w}{\partial y} \right|_{y=0} \tag{26}$$

The local Nusselt quantity, Sherwood quantity, and motile microbe’s density numeral are

$$Nn_x = \frac{xq_n}{D_n(n_w - n_\infty)} = -Re_x^{\frac{1}{2}}\chi'(\xi, 0), \text{ where } q_n = -D_n \left. \frac{\partial n}{\partial y} \right|_{y=0}. \tag{29}$$

$$Nu_x = \frac{xq_w}{\kappa(T_w - T_\infty)} = -Re_x^{\frac{1}{2}}\theta'(\xi, 0), \text{ where } q_w = -\kappa \left. \frac{\partial T}{\partial y} \right|_{y=0}, \tag{27}$$

Fig. 9 Influence of *Nr* on (a) principal flow, (b) subordinate flow, (c) temperature profile, (d) concentration profile, and (e) microorganisms concentration



5 Method of Solution

The Bivariate Spectral Quasi Linearization scheme (BSQLM) was deployed to resolve our assumed modeled nonlinear boundary value problem of two variables specified in Eqs. (20)–(24) and borderline Eq. (25). This method minimizes the computational time and maximizes the results’ accuracy compared to the methods discussed in [45, 46]. The domain of the stream and phases taken by $\xi \in [0, L_t]$ and $\eta \in [0, L_x]$ was renovated to $t \in [-1, 1]$ and $x \in [-1, 1]$ consuming the linear conversions $\eta \in L_x(x + 1)/2$ and $\xi \in L_t(x + 1)/2$, respectively.

The polynomial of the Lagrange interpolation was used to approximate the solution:

$$u(x, t) = \sum_{i=0}^{N_x} \sum_{j=0}^{N_t} \hat{u}(x_i, t_j) L_i(x) L_j(t), \tag{30}$$

Here, toward the x and t lines, we interpolated $u(x, t)$ in particular grid points, which are

$$\{x_i\} = \left\{ \cos \left(\frac{\pi i}{N_x} \right) \right\}_0^{N_x}, \{t_j\} = \left\{ \cos \left(\frac{\pi j}{N_t} \right) \right\}_0^{N_t}. \tag{31}$$

The polynomials of Lagrange cardinal functions $L_i(x)$ are

$$L_i(x) = \prod_{i=0, i \neq j}^{N_x} \frac{x - x_k}{x_i - x_k}, \tag{32}$$

where

$$L_i(x) = \delta_{ik} = \begin{cases} 0, & \text{if } x \neq k \\ 1, & \text{if } x = k. \end{cases} \tag{33}$$

6 Convergence Analysis

The accuracy of the assumed model was confirmed by the graphical representation of the error graph. The convergence and accuracy were numerically analyzed and reflected by the graph. The graph consists of the residual errors norm on the y -axis and the number of iterations on the x -axis. For the flow velocity of primary and secondary variables, the residual error norms are under 10^{-11} after 8 repetitions, while the other variables like thermal, solute, and microbial are less than 10^{-10} after 8 iterations.

The error graph results show that for solving the borderline value problem, BSQLM is an appropriate scheme. Figure 2 demonstrates the residual error norm for existing variables of the model at a diverse number of repetitions.

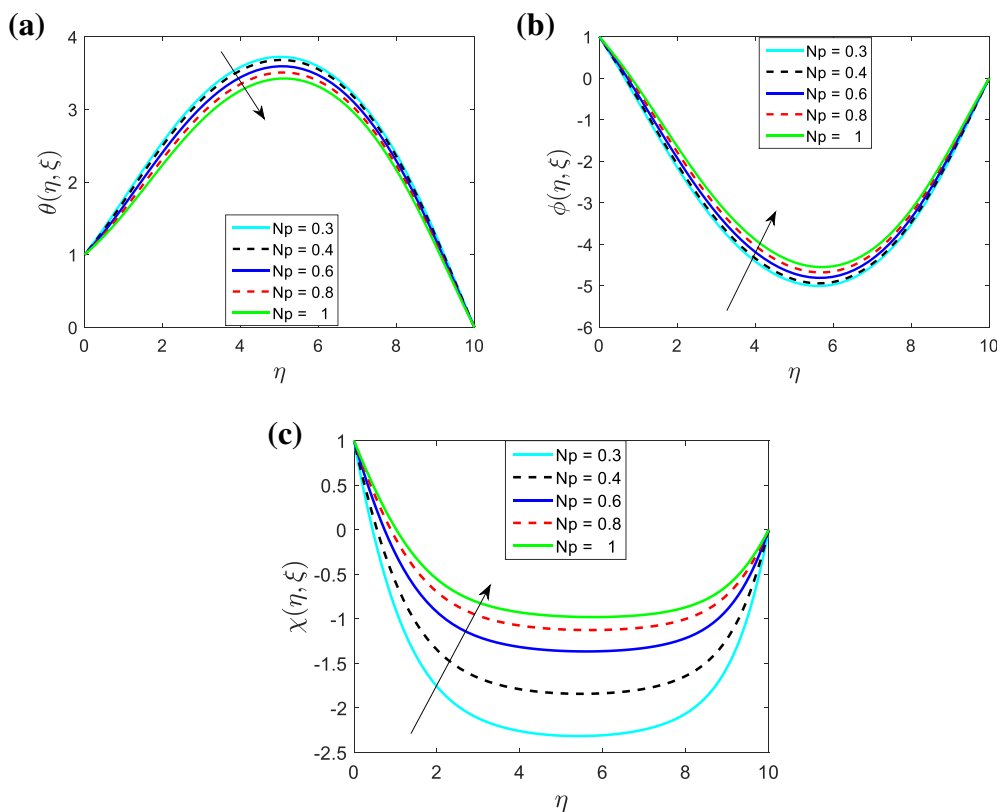
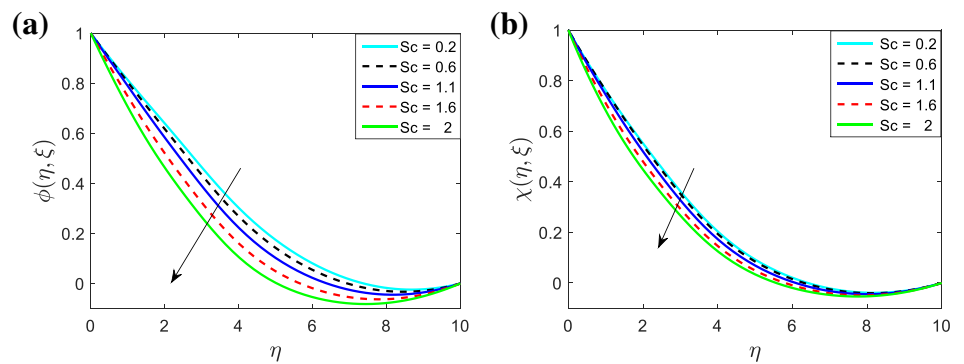


Fig. 10 Influence of N_p on (a) temperature profile, (b) solute profile, and (c) microbial profile

Fig. 11 Influence of Sc on (a) solute profile and (b) microbial profile



The collocation points of our model are represented in Fig. 3 for the principal and subordinate flow, heat, solute, and microorganism outlines.

7 Discussion for the Results

This segment explains the details of our assumed model and the comparison with the related model. This numerically solved set of ODEs derived from the energy, momentum, solutal, accompanied microbial Eqs. (20)–(24), and subjected to the borderline conditions Eq. (25) were analyzed by bivariate quasi-linearization function using MATLAB. We analyzed the results using a bivariate quasi-linearization technique and obtained graphs that show the flow velocity, temperature, concentration, and microbial behavior under various conditions. The outcomes are presented in graphical form for easy understanding.

7.1 Impact of Velocity Fraction Parameter (S)

Here, in Fig 4, we can see that for different values of S , the principal flow and subordinate flow accompanied by temperature profile decrease. The concentration profile of the microbial profile decreases for the growing values of the velocity fraction parameter. The buoyancy forces affect the fluid velocity at the boundary layer. The principal flow is rapidly decreases for higher S , while the subordinate flow was initially enhanced in the range of $0 \leq \eta \leq 0.5$, but then the subordinate swiftness decreases for the range of $\eta \geq 0.5$. Thermal buoyancy affects temperature, and concentration buoyancy affects solute and microbial profiles.

7.2 Impact of Hartmann Number (M)

The impact of the Hartmann number was graphically analyzed in Fig. 5 for different profiles. The dimensionless parameter Hartmann number is the quotient of viscous strength to electromagnetic force. For the growing Hartmann

parameter, the primary flow decreases initially for the range of $0 \leq \eta \leq 3$ while an increase at the boundary layer for the range of $\eta \geq 3$ of the fluid.

The subordinate flow increases initially for the range of $0 \leq \eta \leq 2$ but declines at the borderline layer for the growing Hartmann number layer for the range of $\eta \geq 2$ of the fluid. The enhanced Lorentz force reverses the stream in a frictional drag. The increasing values of the Hartmann number increase the heat profile, while the reverse impact was analyzed for the solute and microbial profile by decreasing.

7.3 Impact of Hall Current (N)

The impact of Hall current affected by the electromagnetic field reflected on various profiles consists in Fig. 6. The increasing values of Hall current N increase the principal flow in the range of $0 \leq \eta \leq 3$ and then decrease at the boundary layer for the range of $\eta \geq 3$ of the fluid, while the subordinate flow initially decreases flow in the range of $0 \leq \eta \leq 1$ after that start increases at the boundary layer for the range of $\eta \geq 1$ of the fluid. However, the heat profile decreases, while the concentration in addition

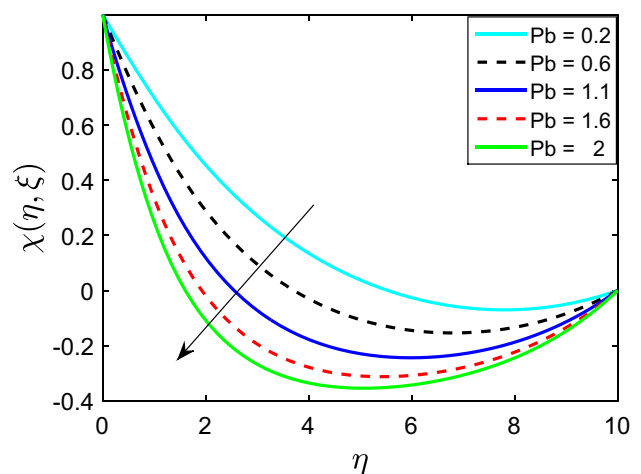


Fig. 12 Influence of Pb on microbial profile

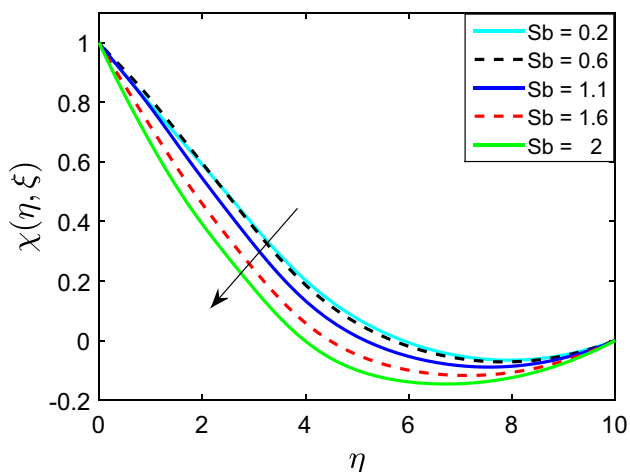


Fig. 13 Influence of *Sb* on microbial profile

to the microbial concentration profile increases for the greater Hall current parameter.

7.4 Impact of Grashof Number (*Gr*)

The impacts of the Grashof number on the principal and subordinate flow, followed by other profiles, are graphically represented in Fig. 7. The Grashof number represents the ratio of buoyant forces to viscous forces. It is used to

determine the flow regime of fluid boundary layers. The enhancement of the *Gr* parameter enhances the principal flow, subordinate flow, solute, and microorganism concentration of the nanofuid while discriminating the temperature outline of the nanofuid.

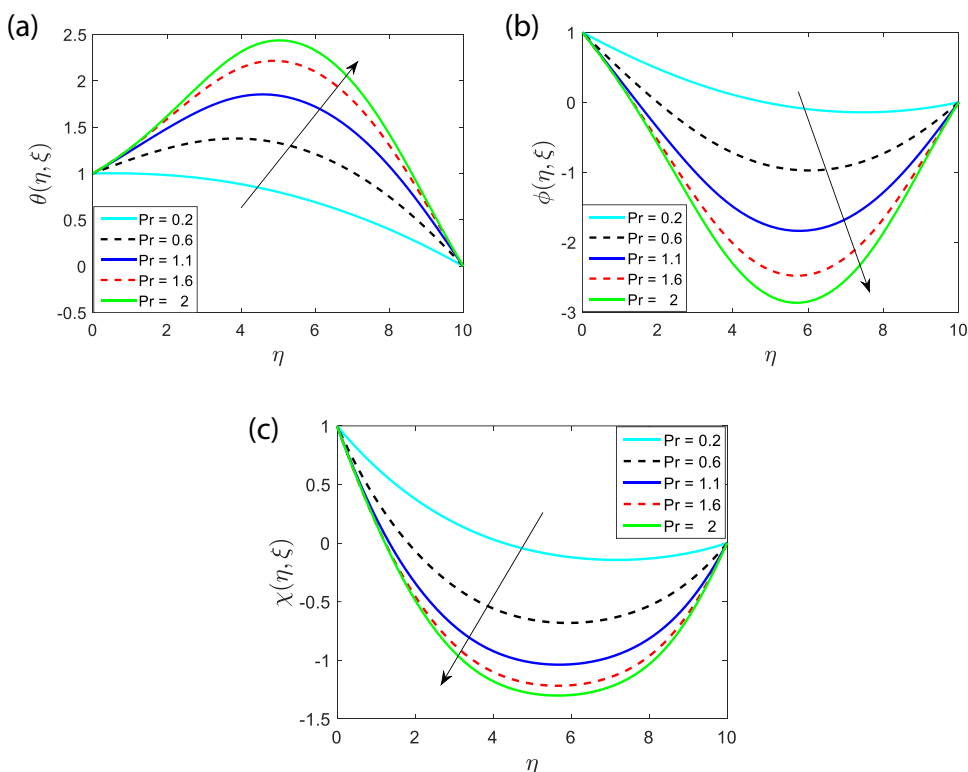
7.5 Impact of Eckert Number (*Ec*)

The impact of Eckert quantity *Ec* on the temperature, solutal, and microbial outlines is graphically represented in Fig. 8. The Eckert number causes the (viscous) dissipation of energy in low-speed flow when combined with the Prandtl number. The enhancement of the parameter discriminates the concentration and microorganism concentration outline of the nanofuid while improving the temperature profile.

7.6 Impact of Buoyancy Ratio Parameter (*Nr*)

The repercussion of the buoyancy ratio parameter *Nr* is graphically studied in Fig. 9. The influence of forced and free convection was measured by the buoyancy ratio parameter. When an external operation is used to maintain or generate the flow, it is known as forced convection, while when the flow is generated because of its internal gradients, like temperature, then it is known as free convection. The enhancement of the parameter increases the

Fig. 14 Influence of *Pr* on (a) temperature profile, (b) solute profile, and (c) microbial profile



principal and subordinate flows accompanied by concentration as well as the microbial concentration of the nano-fluid while declining the temperature outline.

7.7 Impact of Microorganism Brownian Motion Parameter (Np)

The impression of microorganism Brownian motion parameter Np on heat, concentration, and microorganism concentrations was graphically represented in Fig. 10. The Brownian motion parameter with the swimming microorganism affects the usual flow of the fluid. For greater values of Np , it discriminates the heat profile while the concentration and microorganism concentration of the profile are enhanced.

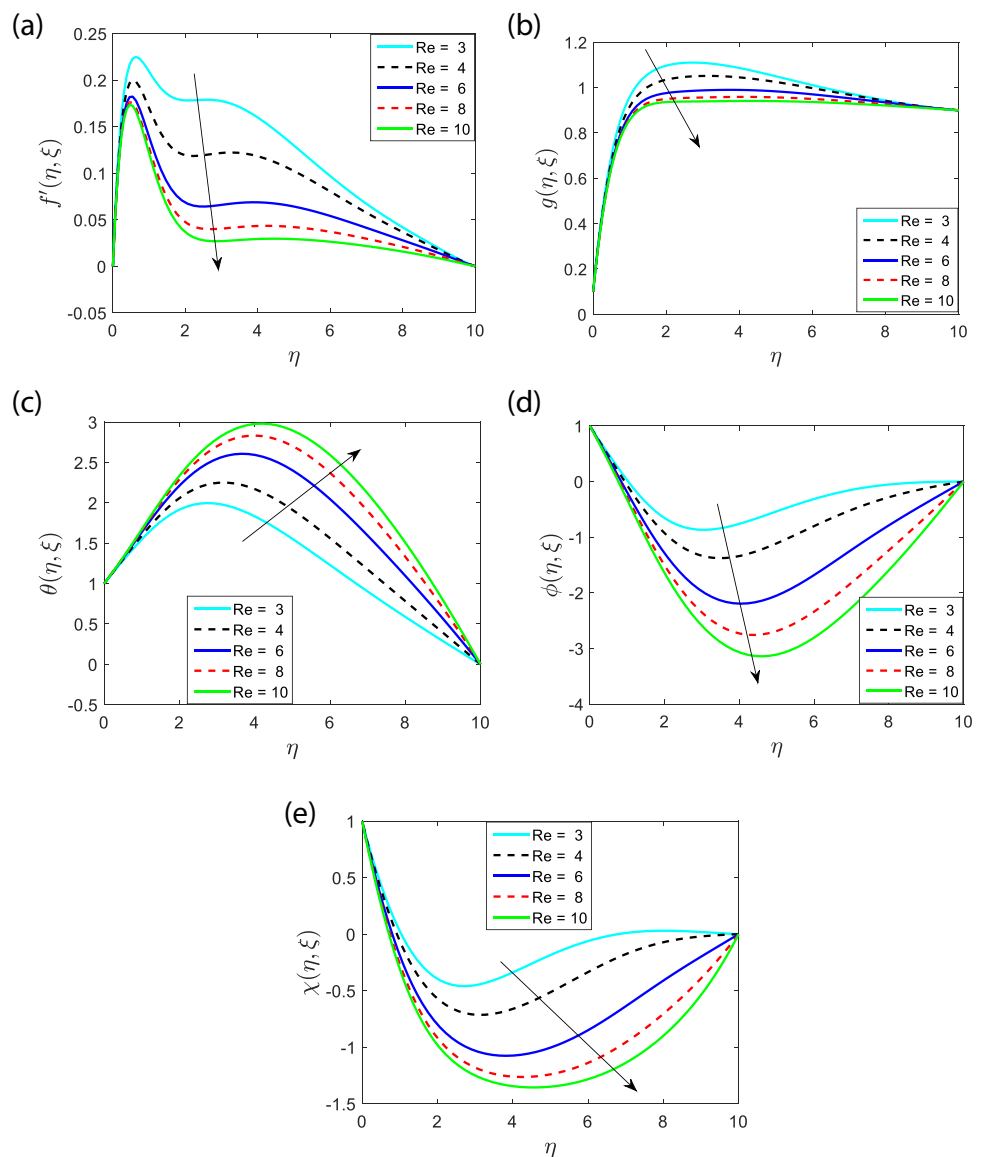
7.8 Impact of Schmidt Number (Sc)

The impressions of Sc Schmidt quantity for the concentration as well as the microbial concentration of the fluid are graphically represented in Fig. 11. This is the ratio of kinematic viscosity (momentum diffusivity) to mass diffusivity, used to characterize fluid flows involving simultaneous momentum, mass diffusion, and convection processes. The improvement of the constraint declines the concentration with microbial concentration profile.

7.9 Impact of Bio-convection Peclet Number (Pb)

The significance of the bio-convection Peclet quantity Pb on the outline of microorganism concentration of the

Fig. 15 Influence of Re on (a) principal flow, (b) subordinate flow, (c) heat profile, (d) solute profile, and (e) microorganisms profile



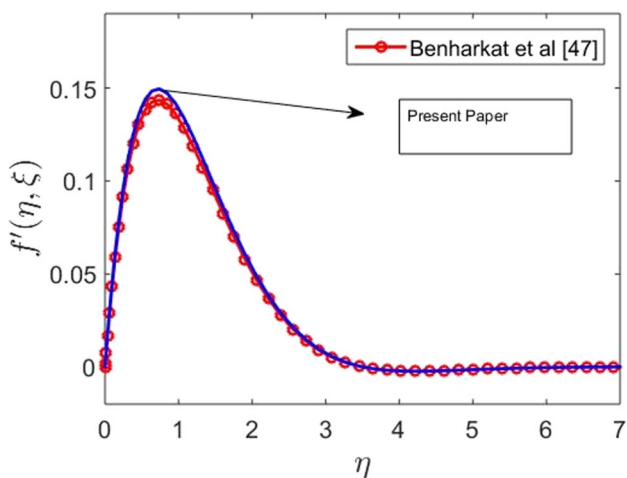


Fig. 16 Comparison graph for the principal velocity profile

liquefied was graphically represented in Fig. 12. This is a dimensionless quantity used to indicate the relative significance of convection and diffusion in a flow system. It is defined as the ratio of diffusive transport to convective transport (advection). Considering the motion of microbes and their diffusion ratio, the bio-convection Peclet number is determined. The escalation of the parameter discriminates the microbe concentration of the fluid.

7.10 Impact of Bio-convection Schmidt Number (*Sb*)

The impression of the bio-convection Schmidt quantity *Sb* on the outline of microorganism concentration of the liquefied was graphically represented in Fig. 13. The parameter increase decreases thermal borderline thickness, increasing Nusselt number and fluid heat profile. The escalation of the parameter discriminates the microbe concentration of the fluid.

7.11 Impact of Prandtl Number (*Pr*)

The impressions of the Prandtl number *Pr* on heat, concentration, and microorganism concentrations were graphically represented in Fig. 14. An increase in the Prandtl number results in a reduction of the thermal boundary layer thickness. The Prandtl number represents the ratio of momentum diffusivity to thermal diffusivity. In heat transfer problems, the Prandtl number governs the relative thickening of the momentum and thermal boundary layers. For greater values of *Pr*, it enhances the heat profile while concentration and microorganism concentration of the profile discriminate.

7.12 Impact of Reynolds Number (*Re*)

Figure 15 reflects that the increasing values of Reynolds numeral *Re* increase the principal and subordinate flow

Table 1 Numerical values of the Nusselt number, Sherwood number, and microbial for different values of engineering parameters

M	Pb	Sb	Np	Nt	Nb	$Re_x^{\frac{1}{2}} \theta'(\xi, 0)$	$Re_x^{\frac{1}{2}} \phi'(\xi, 0)$	$Re_x^{\frac{1}{2}} \chi'(\xi, 0)$
0.2	0.2	0.3	0.5	0.4	0.5	0.12293740	0.58478655	0.12389316
0.5						0.18662044	0.63394051	0.21202719
1.2						0.28810697	0.73919151	0.35358826
0.2	0.2					0.12293740	0.58478655	0.12389316
	0.6					0.12346434	0.58478331	0.14120841
	1.5					0.12473354	0.58496146	0.19828590
0.2	0.2	0.3				0.12293740	0.58478655	0.12389316
		0.8				0.12407477	0.58558531	0.14975628
		1.8				0.12638241	0.58783287	0.36308473
0.2	0.2	0.3	0.5			0.12293740	0.58478655	0.12389316
			0.8			0.13016172	0.58532389	0.12617999
			1.4			0.14429251	0.58612578	0.13022458
0.2	0.2	0.3	0.5	0.4		0.12293740	0.58478655	0.12389316
				0.8		0.15888747	0.58460691	0.15345105
				1.2		0.24538136	0.58535021	0.24499328
0.2	0.2	0.3	0.5	0.4	0.5	0.12293740	0.58478655	0.12389316
					0.8	0.12036001	0.58536127	0.13542924
					1.2	0.11857747	0.58591013	0.14741717

Values in bold indicate that the similar vales for the different values of the different parameters

accompanied by solute as well as microbial outline; however, the heat outline decreases. The high concentration of nanoparticles in nanofluids results in a decrease in velocity and temperature profiles. However, as the fluids come closer to the boundary layer, the increase in Reynolds number leads to an increase in the intermittency of the turbulent fluids, which, in turn, increases the solute and microbial profiles of the fluid.

7.13 Comparison of Graph/Table

The graphical comparison between our model and the reference paper is shown in Fig. 16, confirming our model's validity.

Table 1 presents numerical representative values of the skin friction coefficient, Sherwood number, and microbial density number for variations in different engineering parameters' rotational viscous dissipation. Skin friction drag represents the force per unit area acting tangentially to the solid surface. In this case, the skin friction drag increases for different values of engineering parameters. We observed overall increases in the Sherwood number and microbial density at the boundary layer thickness for different parameters.

8 Conclusion

This rotational viscous dissipative nanofluid flow on a vertically placed mobile plate accompanied by the magnetic field and motile microorganism was considered for this study. The Coriolis and Lorentz forces generated by applying the strong magnetic field on the vertically placed semi-infinite plate, from the buoyancy forces engendered from the concept of coupled occurrence of heat and species-concentration, into an incompressible, steady, and electrically conducting magneto-hydro-dynamic bio-convective rotational nanofluid. The significance of the diverse constraints for the primary and subordinate flow, temperature, solute, and microbe profiles is examined explicitly plus reflected in the encouraging outcomes. The consequences we established in our investigation are summarized as follows.

- The higher value of the wall velocity discriminates the flows in both directions.
- The rise in the Reynolds numbers enhances the heat and discriminates the others.
- Enhancement of the bio-convection Schmidt quantity decreases the microbial outline of the liquefied.
- Enhancement of the bio-convection Peclet numeral decreases the microorganism concentration of the fluid.
- Enrichment of the buoyancy ratio constraint enhances the microbial outline of the fluid.

- Enrichment of the bio-convection Brownian motion constraint decreases the microbe outline of the fluid.
- Advancement of the Schmidt numeral accompanied by the Eckert numeral decreases the concentration of the fluid, while Eckert quantity improves the temperature outline.
- The uptrend of the Hall quantity enhances the concentration as well as microorganism concentration while decreasing the temperature outline of the fluid.

Funding Statement None.

Declarations

Research Involving Humans and Animals Statement None.

Informed Consent None.

Competing interests The authors declare no competing interests.

References

1. Magyari, E., & Keller, B. (1999). Heat and mass transfer in the boundary layers on an exponentially stretching continuous surface. *Journal of Physics D: Applied Physics*, 32(5), 577.
2. Ghaly, A. Y. (2002). Radiation effects on a certain MHD free-convection flow. *Chaos, Solitons & Fractals*, 13, 1843–1850.
3. Chamkha, A. (2004). J. “Unsteady MHD convective heat and mass transfer past a semi-infinite vertical permeable moving plate with heat absorption”. *International Journal of Engineering Science*, 42, 217–230.
4. Mondal, H., Mishra, S., Kundu, P. K., & Sibanda, P. (2020). Entropy generation of variable viscosity and thermal radiation on magnato nanofluid flow with dusty fluid. *Journal of Applied and Computational Mechanics*, 6, 171–182.
5. Mondal, H., Mishra S., & Kundu P. K. (2022). Magneto-hydrodynamics effects over a three-dimensional nanofluid flow through a stretching surface in a porous medium, *Waves in Random and Complex Media*. 1–14. <https://doi.org/10.1080/17455030.2022.2055200>
6. Zueco Jordán, J. (2006). Numerical study of an unsteady free convective magnetohydrodynamic flow of a dissipative fluid along a vertical plate subject to a constant heat flux. *International Journal of Engineering Science*, 44, 1380–1393.
7. Ibrahim, F. S., Elaiw, A. M., & Bakr, A. A. (2008). Effect of the chemical reaction and radiation absorption on the unsteady MHD free convection flow past a semi-infinite vertical permeable moving plate with heat source and suction. *Communications in Nonlinear Science and Numerical Simulation*, 13, 1056–1066.
8. Mohamed, R. A., & Abo-Dahab, S. M. (2009). Influence of chemical reaction and thermal radiation on the heat and mass transfer in MHD micropolar flow over a vertical moving porous plate in

- a porous medium with heat generation. *International Journal of Thermal Sciences*, 48, 1800–1813.
9. Sharma, R., Bhargava, R., & Bhargava, A. (2010). Numerical solution of unsteady MHD convection heat and mass transfer past a semi-infinite vertical porous moving plate using element free Galerkin method. *Computational Materials Science*, 48, 537–543.
 10. Mishra, S., Pal, D., Mondal, H., & Sibanda, P. (2016). On radiative-magnetoconvective heat and mass transfer of a nanofluid past a non-linear stretching surface with Ohmic heating and convective surface boundary condition. *Propulsion and Power Research*, 5(4), 326–337.
 11. Mishra, S., Mondal, H., & Kundu, P. K. (2023). Analysis of Williamson fluid of hydromagnetic nanofluid flow in the presence of viscous dissipation over a stretching surface under radiative heat flux. *International Journal of Applied and Computational Mathematics*, 9(5), 58.
 12. Pop, I., & Watanabe, T. (1994). Hall effects on magnetohydrodynamic free convection about a semi-infinite vertical flat plate. *International Journal of Engineering Science*, 32, 1903–1911.
 13. Chamkha, A. J. (1997). MHD-free convection from a vertical plate embedded in a thermally stratified porous medium with Hall effects. *Applied Mathematical Modelling*, 21, 603–609.
 14. Gorla, R. S. R., Abboud, D. E., & Sarmah, A. (1998). Magneto-hydrodynamic flow over a vertical stretching surface with suction and blowing. *Heat and Mass Transfer*, 34, 121–125.
 15. Duwairi, H. M., & Damseh, R. A. (2004). Magneto-hydrodynamic natural convection heat transfer from radiate vertical porous surfaces. *Heat and Mass Transfer*, 40, 787–792.
 16. Abo-Eldahab, E. M., & El Aziz, M. A. (2005). Viscous dissipation and Joule heating effects on MHD-free convection from a vertical plate with power-law variation in surface temperature in the presence of Hall and ion-slip currents. *Applied Mathematical Modelling*, 29, 579–595.
 17. Saha, L. K., Hossain, M. A., & Gorla, R. S. R. (2007). Effect of Hall current on the MHD laminar natural convection flow from a vertical permeable flat plate with uniform surface temperature. *International Journal of Thermal Sciences*, 46, 790–801.
 18. Das, K. (2011). Effect of chemical reaction and thermal radiation on heat and mass transfer flow of MHD micropolar fluid in a rotating frame of reference. *International Journal of Heat and Mass Transfer*, 54, 3505–3513.
 19. Hayat, T., Qayyum, S., Imtiaz, M., & Alsaedi, A. (2017). Flow between two stretchable rotating disks with Cattaneo-Cristov heat flux model. *Results in Physics*, 7, 126–133.
 20. Ahmed, J., Khan, M., & Ahmad, L. (2019). Swirling flow of Maxwell nanofluid between two coaxially rotating disks with variable thermal conductivity. *Journal of the Brazilian Society of Mechanical Sciences and Engineering*, 41, 97.
 21. Kinyanjui, M., Chaturvedi, N., & Uppal, S. M. (1998). MHD stokes problem for a vertical infinite plate in a dissipative rotating fluid with hall current. *Energy Conversion and Management*, 39, 541–548.
 22. Abdul Maleque, K., & Abdus Sattar, M. (2005). The effects of variable properties and hall current on steady MHD laminar convective fluid flow due to a porous rotating disk. *International Journal of Heat and Mass Transfer*, 48, 4963–4972.
 23. Osalusi, E., Side, J., Harris, R., & Johnston, B. (2007). On the effectiveness of viscous dissipation and Joule heating on steady MHD flow and heat transfer of a Bingham fluid over a porous rotating disk in the presence of Hall and ion-slip currents. *International Communications in Heat and Mass Transfer*, 34, 1030–1040.
 24. Osalusi, E., Side, J., Harris, R., & Clark, P. (2008). The effect of combined viscous dissipation and Joule heating on unsteady mixed convection MHD flow on a rotating cone in a rotating fluid with variable properties in the presence of Hall and ion-slip currents. *International Communications in Heat and Mass Transfer*, 35, 413–429.
 25. Siddiqui, A. M., Rana, M. A., & Ahmed, N. (2008). Effects of hall current and heat transfer on MHD flow of a Burgers' fluid due to a pull of eccentric rotating disks. *Communications in Nonlinear Science and Numerical Simulation*, 13, 1554–1570.
 26. Turkyilmazoglu, M. (2011). Exact solutions for the incompressible viscous magnetohydrodynamic fluid of a rotating-disk flow with Hall current. *International Journal of Non-Linear Mechanics*, 46, 1042–1048.
 27. Takhar, H. S., Chamkha, A. J., & Nath, G. (2002). MHD flow over a moving plate in a rotating fluid with magnetic field, Hall currents and free stream velocity. *International Journal of Engineering Science*, 40, 1511–1527.
 28. Hayat, T., Abbas, Z., & Asghar, S. (2008). Effects of Hall current and heat transfer on rotating flow of a second grade fluid through a porous medium. *Communications in Nonlinear Science and Numerical Simulation*, 13, 2177–2192.
 29. Sharma, K., & Kumar, S. (2023). Impacts of low oscillating magnetic field over ferrofluid flow over upward/downward moving rotating disk with effects of nanoparticle diameter and nanolayer. *Journal of Magnetism and Magnetic Materials*, 575, 17–720.
 30. Kumar, S., & Sharma, K. (2022). Darcy-Forchheimer fluid flow over stretchable rotating disk moving upward/downward with heat source/sink. *Special Topics & Reviews in Porous Media: An International Journal*, 13(4), 33–43.
 31. Kumar, S., & Sharma, K. (2023). Impacts of Stefan blowing on Reiner–Rivlin fluid flow over moving rotating disk with chemical reaction. *Arabian Journal for Science and Engineering*, 48, 2737–2746.
 32. Kumar, S., & Sharma, K. (2022). Mathematical modeling of MHD flow and radiative heat transfer past a moving porous rotating disk with Hall effect. *Multidiscipline Modeling in Materials and Structures* 18(3), 445–458. <https://doi.org/10.1108/mmms-04-2022-0056>
 33. Kumar, S., & Sharma, K. (2022). Entropy optimization analysis of Marangoni convective flow over a rotating disk moving vertically with an inclined magnetic field and nonuniform heat source. *Heat Transfer*, 52(2), 1778–1805.
 34. Kumar, S., & Sharma, K. (2022). Entropy optimized radiative heat transfer of hybrid nanofluid over vertical moving rotating disk with partial slip. *Chinese Journal of Physics*, 77, 861–873.
 35. Abbas, N., Nadeem, S., & Khan, M. N. (2022). Numerical analysis of unsteady magnetized micropolar fluid flow over a curved surface. *Journal of Thermal Analysis and Calorimetry*, 147, 6449–6459.
 36. Abbas, N., & Shatanawi, W. (2022). Heat and mass transfer of micropolar-casson nanofluid over vertical variable stretching Riga sheet. *Energies*, 15(14), 4945.
 37. Khan, A. A., Abbas, N., Nadeem, S., Shi, Q.-H., Malik, M. Y., Ashraf, M., Hussain, S., & A. (2021). Non-Newtonian based micropolar fluid flow over nonlinear stretching cylinder under Soret and Dufour numbers effects. *International communications in Heat and Mass Transfer*, 127, 105571.
 38. Mohammad, F., Zaimi, K., Rashad, A. M., & Nabwey, H. A. (2020). MHD bioconvection flow and heat transfer of nanofluid through an exponentially stretchable sheet. *Symmetry*, 12(5), 692.
 39. Mishra, S., Mondal, H., & Kundu, P. K. (2024). Analysis of activation energy and microbial activity on couple stressed nanofluid with heat generation. *International Journal of Ambient Energy*, 45(1), 1–40. <https://doi.org/10.1080/01430750.2023.2266429>
 40. Mishra, S., Mondal, H., & Kundu, P. K. (2023). Impact of microbial activity and stratification phenomena on generating/absorbing Sutter by nanofluid over a Darcy porous medium. *Journal of Applied and Computational Mechanics*, 9(3), 804–819.

41. Bhatti, M. M., Marin, M., Zeeshan, A., Ellahi, R., & Abdelsalam, S. I. (2020). Swimming of motile gyrotactic microorganisms and nanoparticles in blood flow through anisotropically tapered arteries. *Frontiers in Physics*, 95. <https://doi.org/10.3389/fphy.2020.00095>
42. Alsaedi, A., Khan, M. I., Farooq, M., Gull, N., & Hayat, T. (2017). Magnetohydrodynamic (MHD) stratified bioconvective flow of nanofluid due to gyrotactic microorganisms. *Advanced Powder Technology*, 28(1), 288–298.
43. Avinash, K., Sandeep, N., Makinde, O. D., & Animasaun, I. L. (2017). Aligned magnetic field effect on radiative bioconvection over past a vertical plate with thermophoresis and Brownian motion. *Defect and Diffusion Forum*, 377, 127–140.
44. Mishra, S. R., & Jena, S. (2014). Numerical solution of boundary layer MHD flow with viscous dissipation. *Science World Journal*, 2014, 756498. <https://doi.org/10.1155/2014/756498>
45. Ali, B., Pattnaik, P., Naqvi, R. A., Waqas, H., & Hussain, S. (2021). Brownian motion and thermophoresis effects on bioconvection of rotating Maxwell nanofluid over a Riga plate with Arrhenius activation energy and Cattaneo–Christov heat flux theory. *Thermal Science and Engineering Progress*, 23, 100863.
46. Alhussain, Z. A., Renuka, A., & Muthtamilselvan, M. (2021). A magneto-bioconvective and thermal conductivity enhancement in nanofluid flow containing gyrotactic microorganism. *Case Studies in Thermal Engineering*, 23, 100809.
47. Bagh, A., et al. (2022). Significance of Lorentz and Coriolis forces on dynamics of water based silver tiny particles via finite element simulation. *Ain Shams Engineering Journal*, 13(2), 101572.
48. Chu, Y.-M., et al. (2020). Nonlinear radiative bioconvection flow of Maxwell nanofluid configured by bidirectional oscillatory moving surface with heat generation phenomenon. *Physica scripta*, 95, 105007.
49. Awan, A. U., Majeed, S., Ali, B., & Ali, L. (2022). Significance of nanoparticles aggregation and Coriolis force on the dynamics of Prandtl nanofluid: The case of rotating flow. *Chinese journal of Physics*, 79, 264–272.
50. Bagh, A., Suriya, U. D., Hussein, A. K., Hussain, S., & Naqvi, R. A. (2021). Transient rotating nanofluid flow over a Riga plate with gyrotactic microorganisms, binary chemical reaction and non-Fourier heat flux. *Chinese Journal of Physics*, 7, 732–745.
51. Bagh, A., Siddique, I., Hussain, S., Ali, L., & Baleanu, D. (2022). Boger nanofluid: Significance of Coriolis and Lorentz forces on dynamics of rotating fluid subject to suction/injection via finite element simulation. *Scientific Reports*, 2022(12), 1612.
52. Ahmad, B., et al. (2022). Significance of the Coriolis force on the dynamics of Carreau–Yasuda rotating nanofluid subject to Darcy–Forchheimer and gyrotactic microorganisms. *Mathematics*, 10(16), 2855.
53. Ali, L., Manan, A., & Ali, B. (2022). Maxwell nanofluids: FEM simulation of the effects of suction/injection on the dynamics of rotatory fluid subjected to bioconvection, Lorentz, and Coriolis forces. *Nanomaterials*, 12(19), 3453.
54. Motsa, S., Magagula, V., & Sibanda, P. (2014). A bivariate Chebyshev spectral collocation quasi-linearization method for nonlinear evolution parabolic equations. *The Scientific World Journal*, 2014, 1–13. <https://doi.org/10.1155/2014/581987>
55. Motsa, S. S., Mutua, S. F., & Shateyi, S. (2016). Solving nonlinear parabolic partial differential equations using multidomain bivariate spectral collocation method. In *Nonlinear Systems-Design, Analysis, Estimation and Control*. InTech.
56. Benharrkar, Z., & Bouaziz, M. N. (2018). Coriolis forces and wall velocity effects for MHD rotating fluid past a semi-infinite vertical moving plate. *International journal of applied engineering research*, 13(6), 3361–3368.

Publisher's Note Springer Nature remains neutral with regard to jurisdictional claims in published maps and institutional affiliations.

Springer Nature or its licensor (e.g. a society or other partner) holds exclusive rights to this article under a publishing agreement with the author(s) or other rightsholder(s); author self-archiving of the accepted manuscript version of this article is solely governed by the terms of such publishing agreement and applicable law.